Research Article Vol. 12, No. 7 / 1 Jul 2022 / Optical Materials Express 2805
Optical Materials EXPRESS

Demonstration of the hierarchical arrangement of persistent luminescent microparticles in direct doping-prepared photonic glasses using second-harmonic generation microscopy

SHAMBHAVEE ANNURAKSHITA, VILMA LAHTI, LAETICIA PETIT, AND GODOFREDO BAUTISTA*

Photonics Laboratory, Physics Unit, Tampere University, Korkeakoulunkatu 3, 33720, Tampere, Finland
**godofredo.bautista@tuni.fi*

Abstract: Using three-dimensional (3D) second-harmonic generation (SHG) scanning microscopy, we unravel the formation and distribution of distinct and highly localized persistent luminescent (PeL) microparticles of varied hierarchical levels in glasses prepared using the direct doping method. The PeL microparticles were added in the glasses at different doping temperatures and the glasses were quenched after different dwell time. The SHG maps of the PeL microparticles in the glass, prepared with a doping temperature of 975°C and a dwell time of 3 min, reveal grating-like microscopic domains. This suggests that a large arrangement of PeL crystals spanning several micrometers in three dimensions is manifested by the imbued PeL microparticle. In contrast, the SHG maps of the PeL microparticles inside the glass prepared at doping temperature of 1025°C and dwell time of 10 min, show the existence of single, highly localized and most importantly, submicrometer-sized PeL crystals. These findings substantiate well with the expected behavior of the PeL microparticles in glasses and their physical disintegration in the form of nanoparticles at high doping temperatures and dwell times. The SHG microscopy technique is shown to circumvent the fundamental challenges of traditional and usually destructive imaging methods to detect and visualize PeL nanoparticles in a glass matrix and expected to open a new avenue to evidence the presence of crystals in glasses.

Published by Optica Publishing Group under the terms of the Creative Commons Attribution 4.0 License. Further distribution of this work must maintain attribution to the author(s) and the published article's title, journal citation, and DOI.

1. Introduction

There has been a prevailing interest in the development of photonics glasses especially those inscribed with persistent luminescent (PeL) microparticles (MPs) for many photonics applications. On their own, the PeL MPs exhibit intriguing properties such as long lasting phosphorescence after the excitation [1–3] and long emission lifetimes, allowing the doped glass matrices to be extraordinary useful in various fields such as optoelectronics [4], biomedical sciences [5–7], new light sources [8], and environmental engineering [9]. These functionalities have extensively relied on new process developments to imbue glasses with PeL entities of controllable sizing features at the, e.g., MP [10] and nanoparticle (NP) [11] levels. To fabricate nanosized PeL entities, several fabrication methods, e.g., sol-gel [6], solid phase calcination [12], wet chemicals [13], combustion [14], direct doping method [15], and microencapsulation [16], have been developed. Thus, the advent of technologies to synthesize PeL entity-containing glasses with varied hierarchical domains ranging from millimeter-sized crystallites down to the single NPs opened simultaneously a significant demand to improve and develop techniques to characterize novel photonic glasses and their optical properties.

The most conventional ways to examine the quality of the synthesized PeL entities are accomplished by the use of scanning [17] and transmission electron [18] microscopies, X-ray

#459936 https://doi.org/10.1364/OME.459936
Journal © 2022 Received 30 Mar 2022; revised 2 Jun 2022; accepted 16 Jun 2022; published 27 Jun 2022

Optical Materials EXPRESS

diffraction [19], and energy-dispersive X-ray spectroscopy [20]. These techniques, however, are requiring sample processing, and limited to the characterization of superficial features. Although other optical characterization techniques that rely on linear effects such as luminescence [21,22], Raman [23], and absorption [24,25] have been found to be useful in probing and imaging PeL entities in glasses, these techniques still have drawbacks such as poor spatial resolution, long acquisition times and little depth-discrimination ability. Furthermore, it is impossible to detect and disentangle the light emission from a single PeL NP in an ensemble measurement without investing on extremely sensitive yet costly instruments. The shortcomings of the traditional techniques certainly obstruct the unambiguous probing and possibly exploitable three-dimensional (3D) localization and spatial distribution of embedded PeL NPs in a novel glass matrix.

A well-established imaging technique to study locally and noninvasively a variety of entities including nanocrystals and NPs is based on exploiting the nonlinear optical (NLO) response of the material as a source of image contrast [26,27]. Second-harmonic generation (SHG), which is the simplest NLO phenomenon, is based on the simultaneous scattering of two photons at the fundamental frequency to create a new photon at the doubled frequency [28]. Due to the extreme sensitivity of SHG to spatial symmetries of the samples and/or environment, SHG has been used to reliably investigate and even visualize the spatial symmetries in a plurality of nanocrystalline systems [29–33] and relevant phosphor-containing host matrices [34–35]. More recently, SHG microscopy has been used to unveil the presence of the 3D microscopic-sized crystal domains in a PeL MP that is embedded in glass [36]. Such finding provided the basis of fortifying this nondestructive imaging technique to allow the direct detection and 3D localization of PeL NPs in a glass matrix. The revelation of SHG-active entities at several hierarchical formations would also permit the exploitation of these novel glass composites as promising nonlinear materials with tailorable nonlinear responses at the nanoscale.

Here, we demonstrate the use of SHG microscopy to unambiguously detect and image the hierarchical distribution of PeL entities in a glass matrix. Using 3D scanning microscopy and subsequent SHG validation, we confirm the exclusive formation of SHG-active PeL entities of different hierarchical levels in direct doping method-prepared glass samples. Through our NLO mapping technique, SHG-active PeL nanocrystals in this glass matrix have been detected, validated and visualized nondestructively for the first time.

2. Materials and method

2.1. Sample preparation

Glasses with the composition $50P_2O_5$-$10Na_2O$-40SrO (mol%) were prepared by adding 0.5 wt% of the commercial $SrAl_2O_4:Eu^{2+},Dy^{3+}$ PeL MPs (Jinan G.L. New Materials, China, BG-01, average size of 95 ± 5 µm) in the glass melt using the direct doping method. Detailed description of the direct doping method can be found in [37]. The raw materials $NaPO_3$ and $SrCO_3$ and $(NH_4)_2HPO_4$ were used to prepare $Sr(PO_3)_2$. After melting the 10 g batches at 1050°C for 30 min, the MPs were added at specific doping temperatures of 975, 1000 and 1025°C. The glass was finally cast at varied dwell times (3, 5 and 10 min) after adding the MPs, and finally annealed at 400°C, which is 40°C below the glass transition temperature for 4 h in air. As explained in Ref. [15], almost no decomposition of the PeL MPs in the (975°C – 3 min) glass is expected to occur during the glass preparation whereas few PeL MPs survive the melting process when preparing the (1025°C – 10 min) glass. The glasses prepared with doping temperature – dwell time of (975°C – 3 min), (1000°C – 5 min), and (1025°C – 10 min) were then selected, cut and polished before performing the SHG experiments.

Optical Materials EXPRESS

2.2. NLO microscopy

A custom-built SHG point-scanning microscope was used to study the hierarchical formation of PeL entities in the glasses. The schematic diagram of the SHG microscope that was used in the experiments is shown in Fig. 1. We have previously used this microscope to investigate NLO effects in a variety of samples [36,38–41]. Briefly, the microscope was powered by a femtosecond laser (wavelength of 1060 nm, pulse length of 140 fs, repetition rate of 80 MHz). After intensity attenuation and spatial filtering, the laser beam was expanded to overfill the infinity-corrected microscope objective (numerical aperture of 0.8, magnification of 50×). The same objective was used to focus the incident beam and to collect the optical signals from the sample. The sample was mounted on a computer-controlled piezo-scanning system. The nonlinear signals were separated from the fundamental beam using appropriate dichroic, shortpass (cutoff at 758.2 nm) and bandpass (532 nm ± 9 nm) filters that were mounted before the cooled photomultiplier tube (PMT).

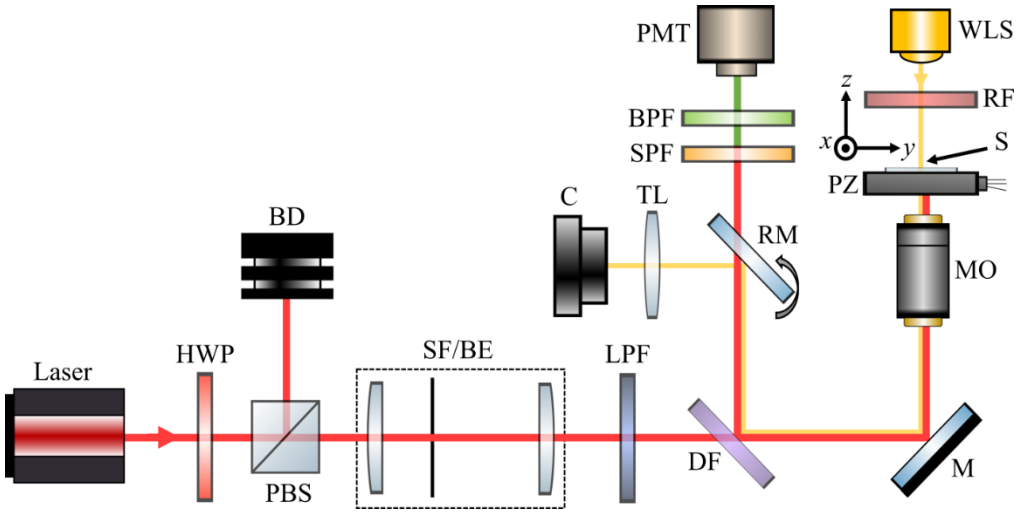

Fig. 1. Schematic diagram of the SHG microscopy setup. The setup includes a femtosecond laser (1060 nm, 140 fs, 80 MHz, Laser), half-wave plate (HWP), polarizing beamsplitter (PBS), beam dump (BD), spatial filter (SF), beam expander (BE), mirror (M), dichroic filter (DF), removable mirror (RM), microscope objective (MO), piezo-scanner (PZ), longpass filter (LPF), shortpass filter (SPF), bandpass filter (BPF), white light source (WLS), red filter (RF), photomultiplier tube (PMT), tube lens (TL), and camera (C).

To create a scanning map, the SHG signals from the sample were collected while the sample was moved in three dimensions with respect to the focused beam (x,y,z), where xy and z correspond to the transversal and axial positions, respectively. These signals were acquired and processed using a custom LabVIEW program that synchronizes the piezo-scanners and the PMT. A SHG map with a resolution of 100 pixels × 100 pixels was acquired from a scanning plane in the focal volume. The pixel dwell time was 50 ms. In all experiments, a linearly-polarized beam (or along the vertical (y) orientation with respect to all SHG maps shown in this paper) at an average incident power of 5 mW was utilized. The input power was controlled using a polarizing beamsplitter and half-wave plate tandem just right after the laser. A longpass filter was used before the microscope to block unwanted nonlinear signals from the optical components. To validate the SHG signals, additional bandpass filters (500 ± 7.5 nm and 560 ± 7 nm) were used. The bandwidth of our femtosecond laser that is operated at 1060 nm is about 8.4 nm (or ± 4.2 nm) so in principle, the integration of nonlinear signals using these bandpass filters centered at

Optical Materials EXPRESS

500 nm, 532 nm and 560 nm with respective bandwidths of 15 nm, 18 nm and 14 nm is sufficient to differentiate the nonlinear signals from the samples. A transmission brightfield imaging arm consisting of a white light source, removable mirror, tube lens and camera was incorporated to view the region of interest in the sample before SHG mapping. A red optical filter was coupled to the white light source to prevent any linear excitation of the sample. All SHG measurements were acquired at room temperature.

3. Results and discussion

$SrAl_2O_4$ belongs to the monoclinic space group $P2_1$ [42] with nonvanishing second-order susceptibility tensor components [28]. SHG microscopy experiments were systematically performed on the three representative PeL MPs-containing glasses prepared using different doping parameters (doing temperature and dwell time). Clear and distinct hierarchical formations of SHG-active PeL entities are exhibited by each glass sample revealing the strong influence of the doping temperature and of the dwell time parameters on the physical properties of the MPs (e.g., size, crystallinity, and dispersion) and hence on the NLO responses of PeL MPs in the host matrix. We first show and discuss the SHG microscopy results from the 975°C – 3 min glass sample. No significant SHG signal from the bulk glass was detected unless a large PeL MP was in the selected scanning area.

Shown in Fig. 2(a) is a brightfield microscopy image of a small (30 μm × 30 μm) area within a large PeL MP found in the (975°C – 3 min) glass taken as an example. The transversal (*xy*) SHG scanning map clearly reveals the existence of many grating-like structures in the PeL MP that are not seen in the brightfield image. Previously, we have verified that such variations in the SHG map arise from material heterogeneities, i.e., presence of differently-oriented crystal domains inside a PeL MP [36]. This result is consistent with our previous finding about the SHG from a large initial cluster of as-prepared PeL MPs [36] suggesting the absence of MP decomposition in this sample. By looking into the upper-right corner of each SHG map [Figs. 2(b)–2(d)], the orientation of domains and SHG signals clearly varied at different focal planes. Based on the SHG map shown in Fig. 2(d), there are at most four distinct PeL MPs in this imaging plane with similar grating-like features that span several micrometers in three dimensions. It is worth noting that the optical contrast of the SHG images is not optimal and can be improved by using circular polarization in order to excite all possible orientations at the focal plane [26]. By changing the bandpass filter before the PMT and fixing the same experimental parameters, the NLO signals at $z = 0$ scanning plane are confirmed to come from the expectedly strong SHG emission wavelength of the PeL MP near 530 nm. This SHG signal is about three to four orders of magnitude higher than the background NLO signals that are allowed by the other bandpass filters [Figs. 2(e)–2(f)]. Essentially, these results clearly demonstrate that SHG microscopy can be used to probe and visualize structured domains inside a PeL MP in a noninvasive manner, i.e., without physically cutting the sample, and consistent with previous work [36].

Next, we performed systematic SHG experiments on the (1000°C – 5 min) glass sample. Upon scanning a typical area that contains PeL MPs [Fig. 3(a)], our SHG scanning maps reveal that the 3D oriented grating-like domains inside the PeL MP are still evident as depicted in the upper-right section of the depth-discriminated SHG maps [Figs. 3(b)– Fig. 3(d)]. Most importantly, 3D SHG mapping unravels the presence of single PeL NPs (marked as NP1 and NP2) in Fig. 3(c). These NPs are actually exclusive only in specific focal planes and absent when the scanned focal plane is changed. Such NLO signals from the NPs are also found to be dominated by SHG (i.e., four orders of magnitude difference) as shown by the weakness of the nonlinear signals depicted in corresponding maps taken at different bandpass filters at the same focal plane [Figs. 3(e),(f)]. Thus, within this glass sample, a mixture of PeL entities composed of grating-like crystal domains and individual PeL NPs is generated and successfully detected by the SHG microscopy technique. This finding corroborates well with the previous findings about the physical properties of this

Optical Materials EXPRESS

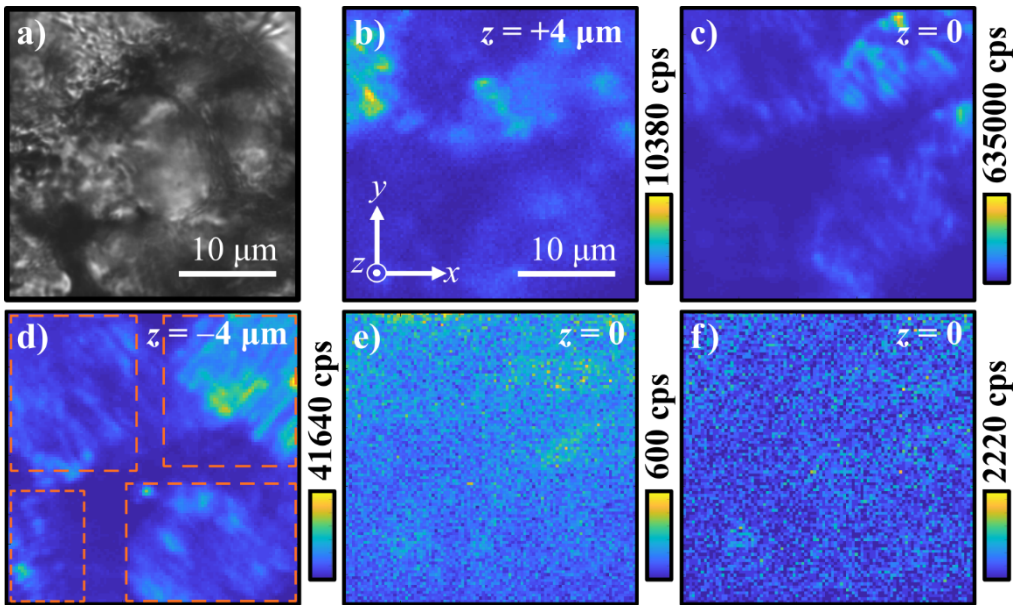

Fig. 2. a) Brightfield image of a small area within a PeL MP in a direct doping-prepared glass sample (975°C – 3 min) at the $z = 0$ scanning plane. b – d) SHG maps of the same area in a) but taken at different focal planes that are separated by 4 µm. In d) 4 representative MPs of varied orientations are marked with dashed squares. Corresponding transversal (xy) SHG scanning map at $z = 0$ scanning plane using e) 500 ± 7.5 nm, and f) 560 ± 7 nm filters before the PMT.

sample, in which the glass exhibits partially disintegrated PeL MPs as a plausible result of the decomposition of the PeL MPs in the glass matrix occurring during the glass preparation [15].

Previous work revealed that significant decomposition of PeL MPs to NPs are expected in the 1025°C – 10 min glass melt [15]. By inspecting the data in Fig. 4, SHG microscopy reveals that inside a single PeL MP, the grating-like SHG distributions are not anymore visible. As such, the NLO signals mostly originate from individual SHG-active PeL NPs or their clusters in three dimensions [Figs. 4(b-e)]. The corresponding line profiles that traverse (along the x-axis) the marked NPs (NP3 and NP4) in Fig. 4(c) show that the emitters are indeed SHG active, highly localized in three dimensions and having sizes that are comparable or smaller than the interrogating excitation focal spot size [Fig. 4(f)] of about 1 µm. To the best of our knowledge, this is the first observation of SHG activity in a nanometer-sized PeL entity in a glass matrix that was prepared using direct doping method. These findings are also evident in the additional SHG microscopy results of these samples (See Figs. S1, S2 and S3 in the Supplement 1).

We take advantage of the inherent noncentrosymmetry of the $SrAl_2O_4$ entities that are imbued in our glasses. As these entities belong to the monoclinic space group $P2_1$, coherent SHG can be driven and more importantly, harnessed as a source of image contrast for microscopy. Since the SHG is generally weak, tight focusing provided by a microscope objective and an ultra-short pulsed laser are necessary to increase the chance of two photons at the fundamental frequency to be scattered instantaneously and to produce a single photon at the SHG frequency. Since the SHG process is tensorial, investigation of the polarization properties (e.g., coherence, sensitivity or directionality) of the hierarchical arrangements of $SrAl_2O_4$ entities could be further studied. Such properties will be challenging to investigate with other optical microscopy techniques that rely on single-photon absorption.

Optical Materials EXPRESS

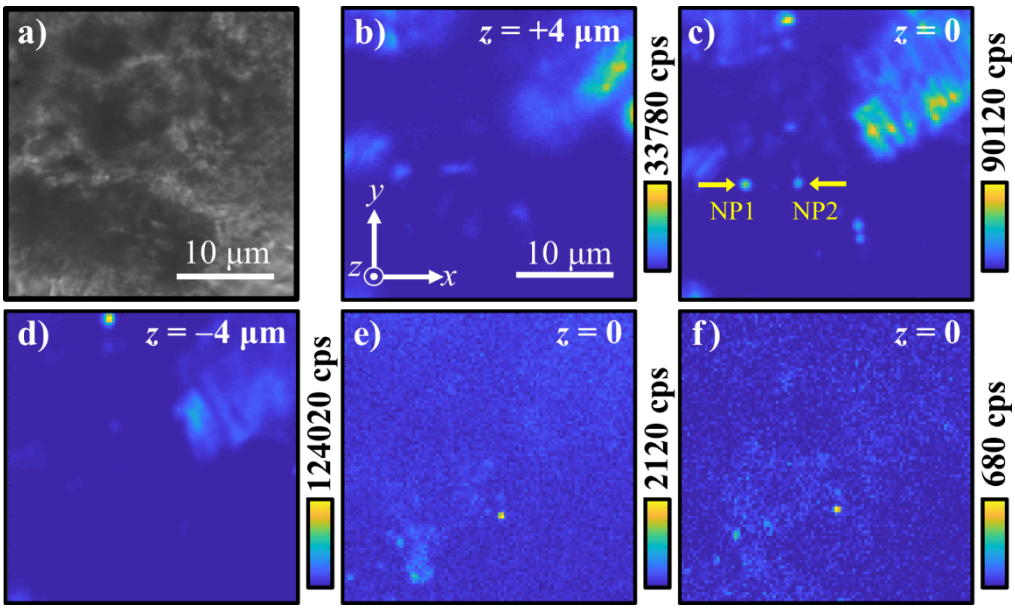

Fig. 3. a) Brightfield image of a small area within a PeL MP in a direct doping-prepared glass sample (1000°C – 5 min) at the $z = 0$ scanning plane. b – d) SHG maps of the same area in a) but taken at different focal planes that are separated by 4 µm. In c) two NPs are marked. Corresponding transversal (xy) SHG scanning map at $z = 0$ scanning plane using e) 500 ± 7.5 nm, and f) 560 ± 7 nm filters before the PMT.

We have previously shown that these samples exhibit strong persistence luminescence signals after stopping the UV excitation at 254 nm [15]. Green persistence luminescence spectra from the samples were found to generally have two broad bands with a maximum at 410 and 490 nm, in which the emission centered at 490 nm has a spectral bandwidth of about 100 nm. The absence of persistence luminescence using our femtosecond excitation is evidenced by the strong SHG at the expected wavelength of 530 nm and the weakness of other nonlinear excitation induced signals near the 500 nm and 560 nm spectral regions (Figs. 2, 3 and 4). This means that the possibility of exciting the persistent luminescence from these samples using the high order harmonics of our excitation at 530 nm, 353 nm and 265 nm is low and not observable in our optical system.

The origin and excitation mechanism of SHG and persistent luminescence are fundamentally different. This fundamental difference could be relaxed due to unwanted and accidental centrosymmetry-inducing effects or symmetry-breaking features (e.g., crystal structure, strain, defects) of the embedded PeL MP and the glass host. In this scenario, it might be possible to probe the SHG and persistent luminescence within the whole glass composite. Although the task is interesting and possibly useful in clarifying the interplay of light-matter (PeL and the glass) interactions, this advance will require new light sources, detectors and setup implementations where the persistent luminescence and SHG are investigated on the same region of the glass sample.

Our work has several implications in photonics and related disciplines that revolve on the interplay of the converging developments in nanoscale nonlinear optics and photonics glass research. First, our experimental results emphasize that SHG microscopy can be used to reliably probe and visualize the hierarchical arrangement of PeL entities in a glass matrix. Most importantly, the technique was able to nondestructively and unambiguously resolve the presence of highly localized PeL NPs that resulted from the disintegration of large PeL MPs in the glass

Optical Materials EXPRESS

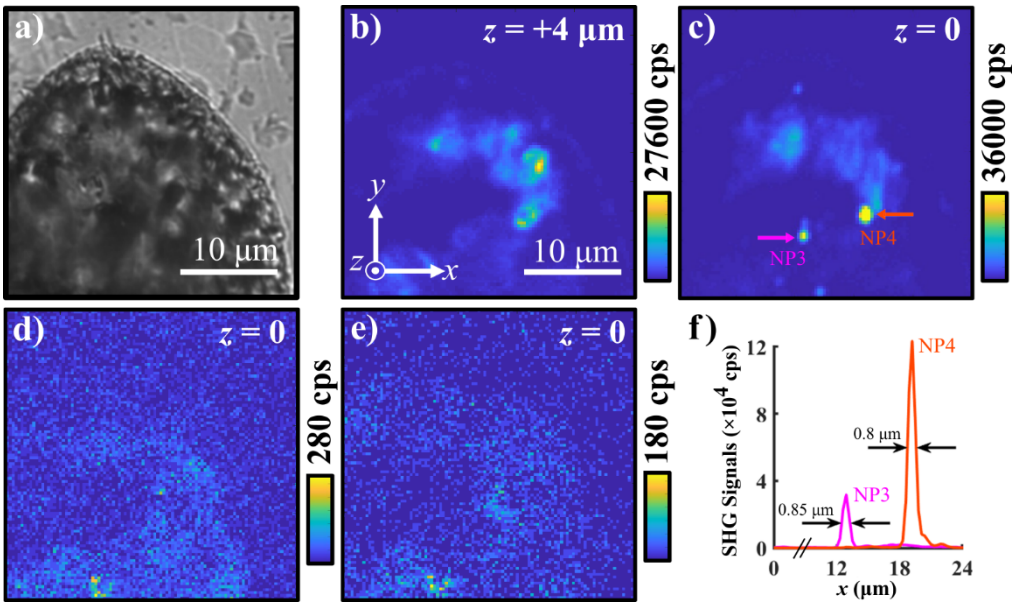

Fig. 4. a) Brightfield image of a small area within a PeL MP in a direct doping-prepared glass sample (1025°C – 10 min) at the $z = 0$ scanning plane. b,c) SHG maps of the same area in a) but taken at different focal planes that are separated by 4 µm. In c) two NPs are marked. Corresponding transversal (xy) SHG scanning map at $z = 0$ scanning plane using d) 500 ± 7.5 nm, and e) 560 ± 7 nm filters before the PMT. f) Averaged SHG intensity profiles acquired from the NPs marked in c). The SHG signals from three adjacent line profiles that run across the NPs along x were averaged. The full width at half maximum for each intensity profile is shown.

matrix at specific direct doping parameters, whose detection and more importantly, imaging remain challenging via traditional characterization techniques. It is worth emphasizing that the traditional techniques are generally surficial, destructive and suffering from low sensitivity, spatial resolution and limited depth-discriminating capability.

Second, the arrangement of PeL MPs in a glass matrix has been already shown to exhibit polarization dependence, which most likely reflects how the PeL MPs are anisotropically packed. It is well-known that the SHG response is tensorial and strongly influenced by the polarization of the incident beam [28]. Further development of the SHG microscopy technique is thus expected to open new ways to study the polarization-dependent SHG response of an individual PeL NP and even visualize its 3D dipole moment using orientation-sensitive techniques [27].

Third, our NLO mapping technique was able to reveal the potential of creating new SHG-active nanoscale sources with tailorable nonlinear responses based on photonics glasses with new functionalities. With more systematic tuning of the direct doping parameters, it is possible to generate a large variety of PeL entities in multiple glasses with controllable size and hence SHG responses at the nanoscale. We also point out that we have only observed the highly localized PeL NPs near the regions where the MPs are located (Figs. 3, 4 and S3 in the Supplement 1). To access if the NPs are numerous and randomly distributed in the glass matrix, new SHG microscopy experiments on many and more importantly large scanning areas need to be done. However, this is a specific technical advance that will require a new setup (e.g., scanning beam approach or widefield illumination) to decrease the scanning times. This research task is certainly interesting but beyond the scope of the present work, where the SHG signals from hierarchical arrangements of PeL are visualized for the first time. The possibility of creating a new SHG-active

Optical Materials EXPRESS

medium or frequency converter comprising of a photonics glass with well-defined, oriented and monodispersed PeL NPs is foreseen.

4. Conclusion

We presented the use of SHG microscopy to probe and visualize the formation and distribution of distinct and highly localized SHG-active PeL crystals in glasses that were prepared using direct doping method. Varied hierarchical levels of PeL entity distribution were revealed in the glasses prepared using different doping temperature (doping temperature and dwell time). The SHG microscopy technique was found to be nondestructive, significantly overcoming the issues of traditional imaging methods to detect and visualize PeL NPs in a glass matrix. The technique shows great potential in complementing our understanding of novel persistent phosphors in glass matrices through the alternative viewpoint using NLO microscopy at the single nanostructure level.

Funding. Academy of Finland (320165, 326418, 328078); Pirkanmaa Regional Fund; Magnus Ehrnroothin Säätiö.

Acknowledgement. S.A. is grateful to Jenny and Antti Wihuri Foundation for the financial support.

Disclosures. The authors declare no conflicts of interest.

Data availability. Data underlying the results presented in this paper are not publicly available at this time, but may be obtained from the authors upon reasonable request.

Supplemental document. See Supplement 1 for supporting content.

References

1. A. Jain, A. Kumar, S. J. Dhoble, and D. R. Peshwe, "Persistent luminescence: an insight," Renewable Sustainable Energy Rev. **65**, 135–153 (2016).
2. J. Hölsä, "Persistent luminescence beats the afterglow: 400 Years of persistent luminescence," Electrochem. Soc. Interface **18**(4), 42–45 (2009).
3. C. C. S. Pedroso, J. M. Carvalho, L. C. V. Rodrigues, J. Hölsä, and H. F. Brito, "Rapid and energy-saving microwave-assisted solid-state synthesis of Pr^{3+}-, Eu^{3+}-, or Tb^{3+}-Doped Lu_2O_3 persistent luminescence materials," ACS Appl. Mater. Interfaces **8**(30), 19593–19604 (2016).
4. J. Ueda, T. Nakanishi, Y. Katayama, and S. Tanabe, "Optical and optoelectronic analysis of persistent luminescence in Eu^{2+}(Dy^{3+} codoped $SrAl_2O_4$ ceramic phosphor," Phys. Status Solidi Curr. Top. Solid State Phys. **9**(12), 2322–2325 (2012).
5. T. Maldiney, A. Bessière, J. Seguin, E. Teston, S. K. Sharma, B. Viana, A. J. J. Bos, P. Dorenbos, M. Bessodes, D. Gourier, D. Scherman, and C. Richard, "The in vivo activation of persistent nanophosphors for optical imaging of vascularization, tumours and grafted cells," Nat. Mater. **13**(4), 418–426 (2014).
6. A. Abdukayum, J. T. Chen, Q. Zhao, and X. P. Yan, "Functional near infrared-emitting Cr^{3+}/Pr^{3+} co-doped zinc gallogermanate persistent luminescent nanoparticles with superlong afterglow for in vivo targeted bioimaging," J. Am. Chem. Soc. **135**(38), 14125–14133 (2013).
7. Q. L. M. De Chermont, C. Chanéac, J. Seguin, F. Pellé, S. Maîtrejean, J. P. Jolivet, D. Gourier, M. Bessodes, and D. Scherman, "Nanoprobes with near-infrared persistent luminescence for in vivo imaging," Proc. Natl. Acad. Sci. U. S. A. **104**(22), 9266–9271 (2007).
8. F. Kang, G. Sun, P. Boutinaud, H. Wu, F. X. Ma, J. Lu, J. Gan, H. Bian, F. Gao, and S. Xiao, "Recent advances and prospects of persistent luminescent materials as inner secondary self-luminous light source for photocatalytic applications," Chem. Eng. J. **403**, 126099 (2021).
9. Y. Li, M. Gecevicius, and J. Qiu, "Long persistent phosphors: from fundamentals to applications," Chem. Soc. Rev. **45**(8), 2090–2136 (2016).
10. N. Ojha, M. Tuomisto, M. Lastusaari, and L. Petit, "Phosphate glasses with blue persistent luminescence prepared using the direct doping method," Opt. Mater. **87**, 151–156 (2019).
11. S. Wu, Y. Li, W. Ding, L. Xu, Y. Ma, and L. Zhang, "Recent advances of persistent luminescence nanoparticles in bioapplications," Nano-Micro Lett. **12**(1), 1–26 (2020).
12. Z. Dai, X. Mao, Q. Liu, D. Zhu, H. Chen, T. Xie, J. Xu, D. Hreniak, M. Nikl, and J. Li, "Effect of dopant concentration on the optical characteristics of Cr^{3+}($ZnGa_2O_4$ transparent ceramics exhibiting persistent luminescence," Opt. Mater. **125**, 112127 (2022).
13. E. Bonturim, L. G. Merízio, R. dos Reis, H. F. Brito, L. C. V. Rodrigues, and M. C. F. C. Felinto, "Persistent luminescence of inorganic nanophosphors prepared by wet-chemical synthesis," J. Alloys Compd. **732**, 705–715 (2018).

Optical Materials EXPRESS

14. N. J. Zúñiga-Rivera, R. García, R. Rodríguez-Mijangos, V. Chernov, R. Meléndrez, M. Pedroza-Montero, and M. Barboza-Flores, "Persistent luminescence, TL and OSL characterization of beta irradiated $SrAl_2O_4$:Eu^{2+}, Dy^{3+} combustion synthesized phosphor," Nucl. Instrum. Methods Phys. Res., Sect. B **326**(3), 99–102 (2014).
15. N. Ojha, H. Nguyen, T. Laihinen, T. Salminen, M. Lastusaari, and L. Petit, "Decomposition of persistent luminescent microparticles in corrosive phosphate glass melt," Corros. Sci. **135**, 207–214 (2018).
16. K. H. Hsu and K. S. Chen, "Photoluminescence of $ZnGa_2O_4$ phosphor prepared by a microencapsulation method," Ceram. Int. **26**(5), 469–473 (2000).
17. K. D. Vernon-Parry, "Scanning electron microscopy: an introduction," III-Vs Review **13**(4), 40–44 (2000).
18. M. Winey, J. B. Meehl, E. T. O'Toole, and T. H. Giddings, "Conventional transmission electron microscopy," Mol. Biol. Cell **25**(3), 319–323 (2014).
19. M. Eckert, P. Knipping, W. H. Bragg, and W. L. Bragg, "Max von Laue and the discovery of X-ray diffraction in 1912," Ann. Phys. **524**(5), A83–A85 (2012).
20. R. Fitzgerald, K. Keil, and K. F. J. Heinrich, "Solid-state energy-dispersion spectrometer for electron-microprobe x-ray analysis," Science **159**(3814), 528–530 (1968).
21. T. Matsuzawa, Y. Aoki, N. Takeuchi, and Y. Murayama, "A new long phosphorescent phosphor with high brightness, $SrAl_2O_4$: Eu^{2+}, Dy^{3+}," J. Electrochem. Soc. **143**(8), 2670–2673 (1996).
22. L. C. V. Rodrigues, R. Stefani, H. F. Brito, M. C. F. C. Felinto, J. Hls, M. Lastusaari, T. Laamanen, and M. Malkamki, "Thermoluminescence and synchrotron radiation studies on the persistent luminescence of $BaAl_2O_4$:Eu^{2+},Dy^{3+}," J. Solid State Chem. **183**(10), 2365–2371 (2010).
23. Y. Zhao, X. Jing, F. Zheng, Y. Liu, and Y. Fan, "Surface-enhanced Raman scattering-active plasmonic metal nanoparticle-persistent luminescence material composite films for multiple illegal dye detection," Anal. Chem. **93**(25), 8945–8953 (2021).
24. K. Pavani, J. S. Kumar, T. Sasikala, B. C. Jamalaiah, H. J. Seo, and L. R. Moorthy, "Luminescent characteristics of Dy^{3+} doped strontium magnesium aluminate phosphor for white LEDs," Mater. Chem. Phys. **129**(1-2), 292–295 (2011).
25. K. Korthout, K. Van Den Eeckhout, J. Botterman, S. Nikitenko, D. Poelman, and P. F. Smet, "Luminescence and x-ray absorption measurements of persistent $SrAl_2O_4$: Eu, Dy powders : Evidence for valence state changes," Phys. Rev. B **84**(8), 085140 (2011).
26. S. Brasselet, "Polarization-resolved nonlinear microscopy: application to structural molecular and biological imaging," Adv. Opt. Photonics **3**(3), 205 (2011).
27. G. Bautista and M. Kauranen, "Vector-field nonlinear microscopy of nanostructures," ACS Photonics **3**(8), 1351–1370 (2016).
28. R. W. Boyd, *Nonlinear Optics* (Academic Press, 2008).
29. A. U. Chowdhury, D. H. Ye, Z. Song, S. Zhang, H. G. Hedderich, B. Mallick, S. Thirunahari, S. Ramakrishnan, A. Sengupta, E. J. Gualtieri, C. A. Bouman, and G. J. Simpson, "Second harmonic generation guided raman spectroscopy for sensitive detection of polymorph transitions," Anal. Chem. **89**(11), 5958–5965 (2017).
30. L. Zhang, W. Kleemann, R. Wang, and M. Itoh, "Second-harmonic study of polar symmetry and domain structure in $SrTi_{18}O_3$," Appl. Phys. Lett. **81**(16), 3022–3024 (2002).
31. S. Cherifi-Hertel, C. Voulot, U. Acevedo-Salas, Y. Zhang, O. Crégut, K. D. Dorkenoo, and R. Hertel, "Shedding light on non-Ising polar domain walls: Insight from second harmonic generation microscopy and polarimetry analysis," J. Appl. Phys. **129**(8), 081101 (2021).
32. J. Kaneshiro, S. Kawado, H. Yokota, Y. Uesu, and T. Fukui, "Three-dimensional observations of polar domain structures using a confocal second-harmonic generation interference microscope," J. Appl. Phys. **104**(5), 054112 (2008).
33. X. Feng, Y. Lun, X. Jiang, J. Qiu, H. Yu, and S. Zhou, "Manipulating nonlinear optical response via domain control in nanocrystal-in-glass composites," Adv. Mater. **33**, 2006482 (2021).
34. D. Hreniak, W. Strek, A. Speghini, M. Bettinelli, G. Boulon, and Y. Guyot, "Infrared induced red luminescence of Eu^{3+} -doped polycrystalline $LiNbO_3$," Appl. Phys. Lett. **88**(16), 161118 (2006).
35. D. M. Krol and J. R. Simpson, "Photoinduced second-harmonic generation in rare-earth-doped aluminosilicate optical fibers," Opt. Lett. **16**(21), 1650 (1991).
36. G. Bautista, L. Kallioniemi, and L. Petit, "Unveiling structured domains of persistent luminescent microparticles using second-harmonic generation microscopy," Opt. Express **28**(18), 25858 (2020).
37. H. Nguyen, M. Tuomisto, J. Oksa, T. Salminen, M. Lastusaari, and L. Petit, "Upconversion in low rare-earth concentrated phosphate glasses using direct $NaYF_4$:Er^{3+}, Yb^{3+} nanoparticles doping," Scr. Mater. **139**, 130–133 (2017).
38. C. Dreser, D. A. Gollmer, G. Bautista, X. Zang, D. P. Kern, M. Kauranen, and M. Fleischer, "Plasmonic mode conversion in individual tilted 3D nanostructures," Nanoscale **11**(12), 5429–5440 (2019).
39. R. Camacho-Morales, G. Bautista, X. Zang, L. Xu, L. Turquet, A. Miroshnichenko, H. H. Tan, A. Lamprianidis, M. Rahmani, C. Jagadish, D. N. Neshev, and M. Kauranen, "Resonant harmonic generation in AlGaAs nanoantennas probed by cylindrical vector beams," Nanoscale **11**(4), 1745–1753 (2019).
40. L. Kallioniemi, S. Annurakshita, and G. Bautista, "Third-harmonic generation microscopy of undeveloped photopolymerized structures," OSA Continuum **3**(11), 2961 (2020).

Optical Materials EXPRESS

41. G. K. Grandhi, A. Matuhina, M. Liu, S. Annurakshita, H. Ali-Löytty, G. Bautista, and P. Vivo, "Lead-free cesium titanium bromide double perovskite nanocrystals," Nanomaterials **11**(6), 1458 (2021).
42. R. E. Rojas-Hernandez, F. Rubio-Marcos, A. Serrano, A. Rakhmatullin, C. Bessada, and J. F. Fernandez, "Unveiling the role of the hexagonal polymorph on $SrAl_2O_4$-based phosphors," RSC Adv. **8**(51), 28918–28927 (2018).

130.230.40.85 {ts '2022-08-03 03:32:11'}